Sustained Oscillations of Grid-forming IBRs under Unbalanced Perturbation: Modal Analysis and EMT Studies

Xinquan Chen, Tao Xue, Ilhan Kocar, Siqi Bu, Maxime Berger

***Abstract*-- Grid-forming inverter-based resources (GFM-IBRs) are considered crucial for power systems with high penetration renewable energy, but their negative sequence behavior under small perturbations remains understudied. This paper proposes a novel decoupled sequence dynamic modeling approach for GFM-IBRs incorporating double-fundamental-frequency negative-sequence components. Using eigenvalue-based stability assessment (EBSA) and electromagnetic transient (EMT) simulation, we reveal that: 1. The proposed modeling approach accurately captures GFM-IBR dynamics under unbalanced small-scale perturbations. 2. Negative-sequence components significantly impact system oscillatory modes. 3. Implementing additional negative-sequence control improves system damping. These findings provide new insights for designing robust GFM-IBR controls and enhancing stability in systems hosting high-penetration renewable systems.**

***Keywords*: Grid-forming controls; inverter-based resources; negative sequence; unbalanced perturbation.**

I. Introduction

GRID-forming (GFM) controls enable inverter-based resources (IBRs) to establish frequency, support voltage, and provide black-start capability for high penetration of renewable energy sources in future power systems [1]−[3]. Prevailing GFM control strategies, such as virtual synchronous machine (VSM) control, droop control, and dispatchable virtual oscillator control (dVOC) [2], [4], use power-synchronization loops (PSLs) and voltage reference generation to mimic traditional synchronous generators (SGs). These are usually implemented with balanced positive-sequence control (BPSC) structures.

Unbalanced disturbances generate sequence components that protective relays detect for correct operation in SG-dominated systems. GFM-IBRs are expected to replicate this behavior under unbalanced conditions [5], allowing negative sequence current flow like conventional SGs. Regarding GFM-IBRs under unbalanced grid conditions, most studies focus on control design for unbalanced fault ride-through [6]−[8], power flow calculations [9], and steady-state analysis [10]. Although positive- and negative-sequence control (PNSC) solutions are proposed for negative-sequence behavior [11], BPSC is still favored for its simplicity. However, there's a critical gap in understanding the dynamics of both strategies under unbalanced small perturbations. As GFM-IBRs become more prevalent, their negative-sequence behavior's impact on system dynamics will likely grow in significance.

Existing studies on the dynamics of GFM-IBRs include various aspects: System-level studies−Interactions between GFL and GFM inverters [13], [14], comparisons of GFL and GFM-based wind farms [15], optimal GFM inverter placement [16], and stability analysis of systems with SGs, GFL-, and GFM-IBRs [12], [17]. Control-level analyses−Advanced virtual-impedance controls [18], [19], adaptive hybrid control [20], power dynamic decoupling control [21], DC-link dynamic regulation [22], and comparisons of VSM, dVOC, and matching control impacts on stability [23]. Inner control loop stability, control damping [24]−[26], SISO stability, and adaptive droop mechanisms have also been studied [27], [28]. However, most studies assume three-phase balanced disturbances, overlooking common unbalanced small perturbations. While conventional GFL-IBRs with BPSC act as open circuits during unbalanced conditions [5], GFM-IBRs show distinct negative sequence dynamics due to their control features. This behavior persists even with BPSC, highlighting the need for further modeling of GFM-IBRs' negative sequence behavior under small, unbalanced perturbations.

Dynamic modeling is crucial for comprehensive modal analysis of GFM-IBR behavior, incorporating control settings. However, most existing models only consider positive-sequence *dq* components, potentially overlooking oscillations caused by negative-sequence components under small, unbalanced perturbations. Recent research has begun addressing this limitation. [29] proposed sequence-decomposed impedance modeling for virtual admittance-based PNSC, examining the impact of sequence component extraction methods on small-signal stability. [30] introduced a decoupled-sequence *dq*0 impedance modeling approach with PNSC, setting negative-sequence voltage references to zero for balanced voltage. While these studies advance PNSC modeling, they don't address the negative-sequence behavior of typical BPSC structures in GFM-IBRs under small, unbalanced perturbations. Given that many GFM-IBRs use the BPSC loop for *dq* components based on the synchronous reference frame (SRF), there remains a gap in understanding and modeling their behavior under these conditions.

Despite the growing importance of GFM-IBRs, there is a significant research gap in understanding their negative

This work was supported in part by PolyU Presidential PhD Fellowship Scheme and GRF of Hong Kong UGC 15229421.

Xinquan Chen, Xue Tao, and Siqi Bu are with Department of Electrical and Electronic Engineering, The Hong Kong Polytechnic University, Hong Kong SAR, China.

Ilhan Kocar is with Polytechnique Montreal, Montreal, QC H3T 1J4, Canada. (e-mail of corresponding author: ilhan.kocar@polymtl.ca).

M. Berger is with the Université du Québec à Rimouski (UQAR), Rimouski, QC G5L 3A1, Canada.

Paper submitted to the International Conference on Power Systems Transients (IPST2025) in Guadalajara, Mexico, June 8-12, 2025.

sequence behavior under unbalanced small perturbations. This paper aims to address this gap with the following specific objectives:

1. Develop a comprehensive decoupled-sequence modeling approach for GFM-IBRs that incorporates double fundamental-frequency negative-sequence components.
2. Validate the proposed model's accuracy in replicating GFM-IBR dynamics under small, unbalanced perturbations.
3. Analyze the oscillatory modes of GFM-IBRs in the negative-sequence system using modal analysis and EMT studies.
4. Evaluate the effectiveness of additional negative-sequence control strategies in improving system damping.

II. Oscillation under Unbalanced Perturbation

Fig. 1 depicts the structure of a typical GFM-IBR plant that incorporates N GFM-IBR units. For each GFM-IBR unit, BPSC strategy is employed to regulate the measurements from IBR hardware and generate modulation signals to drive the voltage source converter (VSC). For the main IBR transformer, the high-voltage (HV) winding uses a grounded Y (Yg) connection, while the medium-voltage (MV) winding uses a D1 connection, with delta voltages lagging Y voltages by 30 degrees. For the IBR unit transformer, the MV winding also uses a D1 connection, while the low-voltage (LV) winding uses a Yg connection.

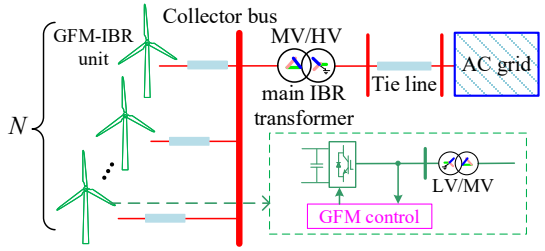

Fig. 1. GFM-IBR plant in power systems

Under unbalanced perturbations, positive-, negative- and zero-sequence components of both voltages and currents are typically present in the AC grid. However, due to the presence of a delta-connected winding in the IBR transformer, only the positive- and negative-sequence components are present on the converter side. Based on the SRF, dq components of an arbitrary variable $\boldsymbol{X}$ in the BPSC loop can be derived as,

$$\boldsymbol{X}_{dq} = \begin{bmatrix} X_\alpha\, cos(\theta) + X_\beta\, sin(\theta) \\ X_\beta\, cos(\theta) - X_\alpha\, sin(\theta) \end{bmatrix} = \boldsymbol{X}_{dq}^{+} + \begin{bmatrix} X_d^{-}\, cos(2\omega t) + X_q^{-}\, sin(2\omega t) \\ X_q^{-}\, cos(2\omega t) - X_d^{-}\, sin(2\omega t) \end{bmatrix} = \boldsymbol{X}_{dq}^{+} + \tilde{\boldsymbol{X}}_{dq}^{-} \quad (1)$$

where $\tilde{\boldsymbol{X}}_{dq}^{-}$ denotes double-fundamental-frequency (2ω) negative-sequence dq components, and θ and ω are the orientation angle and angular frequency, respectively. Superscripts + and – also refer to positive- and negative-sequence components, respectively. For illustration, the diagram of sequence components inside GFM-IBRs under unbalanced perturbations is depicted in Fig. 2. $\boldsymbol{M}$ denotes modulation signals. $\boldsymbol{V}_s$ and $\boldsymbol{I}_s$ are converter terminal voltages and currents, respectively. I_{vsc} denotes the DC-link current on the converter side. R_c and L_c are the choke resistance and inductance, respectively. The shunt filter is modeled with capacitor C_f. In subscript, *set* refers to setpoints, while *dc* denotes DC-link components.

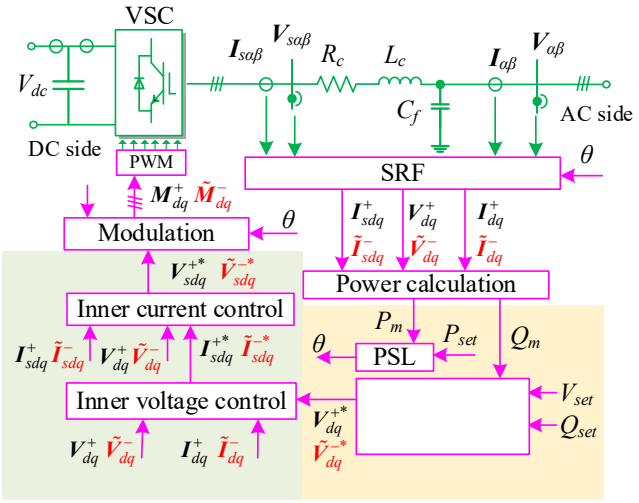

Fig. 2. Sequence components within the typical GFM BPSC system under unbalanced perturbations

III. Generic Decoupled-Sequence Dynamic Modeling for GFM-IBRs

A. Generic Decoupled-Sequence Modeling Structure

To evaluate the influence of 2ω negative-sequence components within GFM controls, a decoupled-sequence modeling approach for GFM-IBRs is designed, which can be represented by a unified time-domain model, as follows

$$\begin{cases} \boldsymbol{x}(t) = \left[\boldsymbol{x}_{dq}^{+}(t) \quad \boldsymbol{x}_{dq}^{-}(t) \quad \boldsymbol{x}_s(t) \quad \boldsymbol{x}_{dc}(t)\right]^T \\ \dot{\boldsymbol{x}}(t) = f(\boldsymbol{x}(t)) \end{cases} \quad (2)$$

where $\boldsymbol{x}_{dq}^{+}(t)$ and $\boldsymbol{x}_{dq}^{-}(t)$ represent the state variables of the positive- and negative-sequence dq components, respectively. $\boldsymbol{x}_s(t)$ and $\boldsymbol{x}_{dc}(t)$ represent the state variables of the GFM control system and DC system, respectively.

B. GFM BPSC System

1) GFM primary control:

The VSM control emulates the rotor motion and primary frequency regulation of SGs, enabling GFM-IBRs to exhibit the active power versus frequency droop mechanism and swing behavior, as given by,

$$\begin{cases} \dot{\omega} = \frac{(P_{set} - x_P)}{J\omega_n} + \frac{D_p(\omega_n - \omega)}{J} \\ \dot{x}_P = \omega_f(P_m - x_P) \end{cases} \quad (3)$$

where J is the virtual inertia constant, D_p is the droop gain, and ω_n and ω_f are the nominal frequency and cut-off frequency, respectively. x_P is a state variable of the low-pass filter of active power. Under unbalanced grid conditions, the d-axis voltage is given by,

$$V_d = V_d^{+} + \tilde{V}_d^{-} = V_d^{+} + V_d^{-}\, cos(2\omega t) + V_q^{-}\, sin(2\omega t) \quad (4)$$

Then, the virtual flux leakage is derived as,

$$\psi_M = \psi_M^{+} + \tilde{\psi}_M^{-} \quad (5)$$

$$\begin{cases}\psi_M^+ = k_{pvac}\underbrace{(V_{set}-V_d^+)}_{\dot{x}_V^+} + k_{ivac}x_V^+ \\ \tilde{\psi}_M^- = k_{pvac}\underbrace{(0-\tilde{V}_d^-)}_{\dot{\tilde{x}}_V^-} + k_{ivac}\tilde{x}_V^-\end{cases} \tag{6}$$

where k_{pvac} and k_{ivac} are the PI-controller gains. x_V is a state variable of the PI controller for generating virtual flux leakage. On this basis, the virtual voltage references are determined as,

$$\begin{cases}\boldsymbol{V}_{dq}^{+*} = \mathbf{T}_{dq}(\theta)\mathbf{T}_{\alpha\beta}\omega\psi_M^+ sin(\hat{\theta}) \\ \tilde{\boldsymbol{V}}_{dq}^{-*} = \mathbf{T}_{dq}(\theta)\mathbf{T}_{\alpha\beta}\omega\tilde{\psi}_M^- sin(\hat{\theta}) \\ sin(\hat{\theta}) = \left[sin(\theta) \quad sin(\theta-\frac{2\pi}{3}) \quad sin(\theta-\frac{4\pi}{3})\right]^T\end{cases} \tag{7}$$

where

$$\begin{cases}\mathbf{T}_{dq}(\theta) = \begin{bmatrix} cos(\theta) & sin(\theta) \\ -sin(\theta) & cos(\theta)\end{bmatrix} \\ \mathbf{T}_{\alpha\beta} = \sqrt{\frac{2}{3}}\begin{bmatrix}1 & \frac{-1}{2} & \frac{-1}{2} \\ 0 & \frac{\sqrt{3}}{2} & \frac{-\sqrt{3}}{2}\end{bmatrix}\end{cases} \tag{8}$$

The droop control replicates the speed droop characteristic of the synchronous generator (SG) governor and balances deviations in power injection. Frequency regulation is modeled with (9) and voltage reference regulation is modeled with (10) and (11), where m_p is the droop gain.

$$\omega = \omega_n - m_p(P_m - P_{set}) \tag{9}$$

$$\begin{cases}V_d^* = V_d^{+*} + \tilde{V}_d^{-*} \\ V_q^* = 0\end{cases} \tag{10}$$

$$\begin{cases}V_d^{+*} = k_{pvac}\underbrace{(V_{set}-V_d^+)}_{\dot{x}_V^+} + k_{ivac}x_V^+ \\ \tilde{V}_d^{-*} = k_{pvac}\underbrace{(0-\tilde{V}_d^-)}_{\dot{\tilde{x}}_V^-} + k_{ivac}\tilde{x}_V^-\end{cases} \tag{11}$$

The dVOC function regulates active and reactive power separately, thus obtaining the amplitude and phase of virtual voltage references [4], as follows:

Frequency regulation:

$$\begin{cases}\omega = \omega_n + \kappa_1(\frac{P_{set}}{(V_{set})^2} - \frac{x_P}{(V_d^*)^2}) \\ \dot{x}_P = \omega_f(P_m - x_P)\end{cases} \tag{12}$$

Voltage reference generation:

$$\begin{cases}\dot{V}_d^* = V_d^*\left(\kappa_1\left(\frac{Q_{set}}{(V_{set})^2} - \frac{x_Q}{(V_d^*)^2}\right) + \frac{\kappa_2(V_{set}^2-(V_d^*)^2)}{V_{set}^2}\right) \\ \dot{x}_Q = \omega_f(Q_m - x_Q)\end{cases} \tag{13}$$

where κ_1 and κ_2 denote synchronization gains. x_Q is a state variable of the low-pass filter of reactive power. Since the dVOC regulates voltage references via the reactive power, $\tilde{V}_d^-$ does not affect voltage reference generation.

2) GFM inner control:

The inner control loop consists of the inner voltage and current control. Typical dual closed-loop design controllers with feedforward terms are employed. Under unbalanced grid conditions, the measured *dq* voltages and currents are given by,

$$\boldsymbol{X} = \{I, V, I_s\} \tag{14}$$

$$\boldsymbol{X}_{dq} = \boldsymbol{X}_{dq}^+ + \tilde{\boldsymbol{X}}_{dq}^- = \begin{bmatrix}X_d^+ + X_d^- cos(2\omega t) + X_q^- sin(2\omega t) \\ X_q^+ + X_q^- cos(2\omega t) - X_d^- sin(2\omega t)\end{bmatrix} \tag{15}$$

The formulas of inner voltage control are derived as,

$$\begin{cases}\boldsymbol{I}_{sdq}^{+*} = k_{iv}\boldsymbol{x}_{Vdq}^+ + k_{pv}\underbrace{(\boldsymbol{V}_{dq}^{+*}-\boldsymbol{V}_{dq}^+)}_{\dot{\boldsymbol{x}}_{Vdq}^+} + \underbrace{\boldsymbol{\gamma}C_f\boldsymbol{V}_{dq}^+ + \boldsymbol{I}_{dq}^+}_{\text{feedforward}} \\ \tilde{\boldsymbol{I}}_{sdq}^{-*} = k_{iv}\tilde{\boldsymbol{x}}_{Vdq}^- + k_{pv}\underbrace{(\tilde{\boldsymbol{V}}_{dq}^{-*}-\tilde{\boldsymbol{V}}_{dq}^-)}_{\dot{\tilde{\boldsymbol{x}}}_{Vdq}^-} + \underbrace{\boldsymbol{\gamma}C_f\tilde{\boldsymbol{V}}_{dq}^- + \tilde{\boldsymbol{I}}_{dq}^-}_{\text{feedforward}}\end{cases} \tag{16}$$

where $\boldsymbol{\gamma} = \begin{bmatrix}0 & \omega \\ -\omega & 0\end{bmatrix}$ and k_{pv} and k_{iv} are PI-controller gains of the inner voltage control. $\boldsymbol{x}_{Vdq}$ denotes state variables of the PI controller of inner voltage control. The formulas of inner current control are derived as,

$$\begin{cases}\boldsymbol{V}_{sdq}^{+*} = k_{pi}\underbrace{(\boldsymbol{I}_{dq}^{+*}-\boldsymbol{I}_{dq}^+)}_{\dot{\boldsymbol{x}}_{Idq}^+} + k_{ii}\boldsymbol{x}_{Idq}^+ + \underbrace{\boldsymbol{\gamma}L_c\boldsymbol{I}_{dq}^+ + \boldsymbol{V}_{dq}^+}_{\text{feedforward}} \\ \tilde{\boldsymbol{V}}_{sdq}^{-*} = k_{pi}\underbrace{(\tilde{\boldsymbol{I}}_{dq}^{-*}-\tilde{\boldsymbol{I}}_{dq}^-)}_{\dot{\tilde{\boldsymbol{x}}}_{Idq}^-} + k_{ii}\tilde{\boldsymbol{x}}_{Idq}^- + \underbrace{\boldsymbol{\gamma}L_c\tilde{\boldsymbol{I}}_{dq}^- + \tilde{\boldsymbol{V}}_{dq}^-}_{\text{feedforward}}\end{cases} \tag{17}$$

where k_{pi} and k_{ii} are the PI-controller gains of the inner current control. $\boldsymbol{x}_{Idq}$ denotes state variables of the PI controller of inner voltage control. The modulation signals are generated by the inner current control, as follows:

$$\begin{cases}\boldsymbol{M}_{dq}^+ = \frac{2}{V_{dc}}\boldsymbol{V}_{sdq}^{+*} \\ \tilde{\boldsymbol{M}}_{dq}^- = \frac{2}{V_{dc}}\tilde{\boldsymbol{V}}_{sdq}^{-*}\end{cases} \tag{18}$$

$$\boldsymbol{M}_{dq}^- = \begin{bmatrix}\tilde{M}_d^- cos(2\omega t) - \tilde{M}_q^- sin(2\omega t) \\ \tilde{M}_q^- cos(2\omega t) + \tilde{M}_d^- sin(2\omega t)\end{bmatrix} \tag{19}$$

C. GFM PNSC System

For regulating positive- and negative-sequence components independently, a GFM PNSC structure is employed, as illustrated in [30]. In PNSC, sequence component extraction methods, such as decoupled double SRF (DDSRF) [31] or quarter-cycle phase delay (QCPD) method [29], can be utilized to eliminate the effects of 2ω negative-sequence components of voltages and currents. In this way, the positive- and negative-sequence components can be separated. Hence, for PNSC, the 2ω negative-sequence components $\tilde{\boldsymbol{X}}_{dq}^-$ equal zero in (3)–(19). To address these uncontrolled negative-sequence components, two types of negative-sequence control solutions for GFM-IBRs are considered in this paper, i.e., the balanced voltage control strategy [32] given by (20) and balanced current control strategy [33] given by (21).

$$\begin{cases}\boldsymbol{V}_{dq}^{-*} = 0 \\ \boldsymbol{I}_{sdq}^{-*} = (k_{pv} + \frac{k_{iv}}{s})(\boldsymbol{V}_{dq}^{-*} - \boldsymbol{V}_{dq}^-) + \boldsymbol{\gamma}C_f\boldsymbol{V}_{dq}^- + \boldsymbol{I}_{dq}^- \\ \boldsymbol{V}_{sdq}^{-*} = (k_{pi} + \frac{k_{ii}}{s})(\boldsymbol{I}_{sdq}^{-*} - \boldsymbol{I}_{sdq}^-) + \boldsymbol{\gamma}L_c\boldsymbol{I}_{sdq}^- + \boldsymbol{V}_{dq}^- \\ \boldsymbol{M}_{dq}^- = \frac{2}{V_{dc}}\boldsymbol{V}_{sdq}^{-*}\end{cases} \tag{20}$$

$$\begin{cases}\boldsymbol{I}_{sdq}^{-*} = 0 \\ \boldsymbol{V}_{sdq}^{-*} = (k_{pi} + \frac{k_{ii}}{s})(\boldsymbol{I}_{sdq}^{-*} - \boldsymbol{I}_{sdq}^-) + \boldsymbol{\gamma}L_c\boldsymbol{I}_{sdq}^- + \boldsymbol{V}_{dq}^- \\ \boldsymbol{M}_{dq}^- = \frac{2}{V_{dc}}\boldsymbol{V}_{sdq}^{-*}\end{cases} \tag{21}$$

D. AC and DC systems

Since the paper focuses on the negative-sequence behavior of GFM-IBRs on the AC side, the DC system can be simplified to a DC-voltage-controlled current source, as given by,

$$\begin{cases} I_{dcset} = k_{Vdc}(V_{dcset} - V_{dc}) \\ \dot{I}_{dc} = \frac{I_{dcset} - I_{dc}}{T_{dc}} \\ \dot{V}_{dc} = \frac{I_{dc} - I_{vsc}}{C_{dc}} = \frac{I_{dc} - \frac{1}{2}(\boldsymbol{M}_{\alpha\beta})^T \boldsymbol{I}_{s\alpha\beta}}{C_{dc}} \end{cases} \tag{22}$$

where T_{dc} and k_{Vdc} denote the time delay constant and DC voltage control gain, respectively. For the AC system in Fig. 2, positive- and negative-sequence differential equations in dq coordinates are derived as,

$$\begin{cases} \dot{\boldsymbol{I}}^+_{sdq} = \frac{\boldsymbol{V}^+_{sdq} - R_c \boldsymbol{I}^+_{sdq} - \boldsymbol{V}^+_{dq}}{L_c} + \boldsymbol{\gamma} \boldsymbol{I}^+_{sdq} \\ \dot{\boldsymbol{I}}^-_{sdq} = \frac{\boldsymbol{V}^-_{sdq} - R_c \boldsymbol{I}^-_{sdq} - \boldsymbol{V}^-_{dq}}{L_c} + \boldsymbol{\gamma} \boldsymbol{I}^-_{sdq} \end{cases} \tag{23}$$

$$\begin{cases} \dot{\boldsymbol{V}}^+_{dq} = \frac{\boldsymbol{I}^+_{sdq} - \boldsymbol{I}^+_{dq}}{C_f} + \boldsymbol{\gamma} \boldsymbol{V}^+_{dq} \\ \dot{\boldsymbol{V}}^-_{dq} = \frac{\boldsymbol{I}^-_{sdq} - \boldsymbol{I}^-_{dq}}{C_f} + \boldsymbol{\gamma} \boldsymbol{V}^-_{dq} \end{cases} \tag{24}$$

E. Linearization

By linearizing the proposed model $\dot{\boldsymbol{x}}(t) = f(\boldsymbol{x}(t))$ at steady-state equilibrium, decoupled-sequence small-signal models of GFM-IBRs are derived as follows:

$$\begin{cases} \Delta \boldsymbol{x} = [\Delta \boldsymbol{x}^+_{dq} \quad \Delta \boldsymbol{x}^-_{dq} \quad \Delta \boldsymbol{x}_s \quad \Delta \boldsymbol{x}_{dc}]^T \\ \Delta \dot{\boldsymbol{x}} = \boldsymbol{A} \Delta \boldsymbol{x} + \boldsymbol{B} \Delta \boldsymbol{u} \end{cases} \tag{25}$$

where $\boldsymbol{A}$ denotes the state-space matrix. $\boldsymbol{B}$ denotes the input matrix. The state variables are then given by

$$\Delta \boldsymbol{x}^+_{dq} = \left[\underbrace{\Delta \boldsymbol{I}^+_{sdq} \quad \Delta \boldsymbol{V}^+_{dq}}_{\text{AC system}} \quad \underbrace{\Delta \boldsymbol{x}^+_{Vdq} \quad \Delta \boldsymbol{x}^+_{Idq}}_{\text{Inner control}}\right]^T \tag{26}$$

$$\Delta \boldsymbol{x}^-_{dq} = \left[\underbrace{\Delta \boldsymbol{I}^-_{sdq} \quad \Delta \boldsymbol{V}^-_{dq}}_{\text{AC system}} \quad \underbrace{\Delta \boldsymbol{x}^-_{Vdq} \quad \Delta \boldsymbol{x}^-_{Idq}}_{\text{Inner control}}\right]^T \tag{27}$$

$$\Delta \boldsymbol{x}_{dc} = \left[\underbrace{\Delta \boldsymbol{I}_{dc} \quad \Delta \boldsymbol{V}_{dc}}_{\text{DC system}}\right]^T \tag{28}$$

For the VSM control strategy (GFM_{VSM}),

$$\Delta \boldsymbol{x}_s = [\Delta \boldsymbol{x}^+_V \quad \Delta \boldsymbol{x}^-_V \quad \Delta\theta \quad \Delta\omega \quad \Delta x_P]^T \tag{29}$$

$$\Delta \boldsymbol{u} = \left[\Delta \boldsymbol{I}^+_{dq} \quad \Delta \boldsymbol{I}^-_{dq} \quad \underbrace{\Delta P_{set} \quad \Delta V_{set}}_{\text{VSM control input}}\right]^T \tag{30}$$

For the droop control strategy ($\text{GFM}_{\text{droop}}$),

$$\Delta \boldsymbol{x}_s = [\Delta \boldsymbol{x}^+_V \quad \Delta \boldsymbol{x}^-_V \quad \Delta\theta \quad \Delta x_P]^T \tag{31}$$

$$\Delta \boldsymbol{u} = \left[\Delta \boldsymbol{I}^+_{dq} \quad \Delta \boldsymbol{I}^-_{dq} \quad \underbrace{\Delta P_{set} \quad \Delta V_{set}}_{\text{droop control input}}\right]^T \tag{32}$$

For the dVOC strategy (GFM_{dVOC}),

$$\Delta \boldsymbol{x}_s = [\Delta\theta \quad \Delta V^*_d \quad \Delta x_P \quad \Delta x_Q]^T \tag{33}$$

$$\Delta \boldsymbol{u} = \left[\Delta \boldsymbol{I}^+_{dq} \quad \Delta \boldsymbol{I}^-_{dq} \quad \underbrace{\Delta P_{set} \quad \Delta Q_{set} \quad \Delta V_{set}}_{\text{dVOC input}}\right]^T \tag{34}$$

Overall, the proposed modeling approach provides a detailed illustration of the regulation of negative-sequence components within GFM-IBRs. The derived state-space matrix can be used to further analyze the impact of negative-sequence components on system dynamics through modal analysis.

IV. Dynamic Model vs. EMT Model

To validate the proposed decoupled-sequence modeling approach of GFM-IBRs, a 9-bus test system is developed in Matlab/Simulink as an EMT model. The original 9-bus model can be found in [4]. For validation purposes, EMT simulations are conducted to produce detailed power system transients across various timescales. The parameter configuration of GFM-IBRs is listed in Table AI of the Appendix.

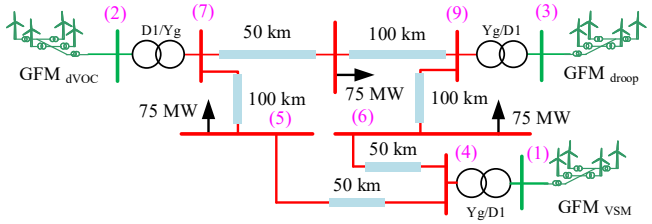

Fig. 3. Test system: 100% GFM-IBR-dominated system

In the test system, GFM-IBR operates at P_m=75 MW. For illustration, when t=15 s, a 75 MW unbalanced load is applied at Bus (6), resulting in the imbalance of grid voltages and currents. The negative-sequence components of grid voltages are shown in Fig. 4.

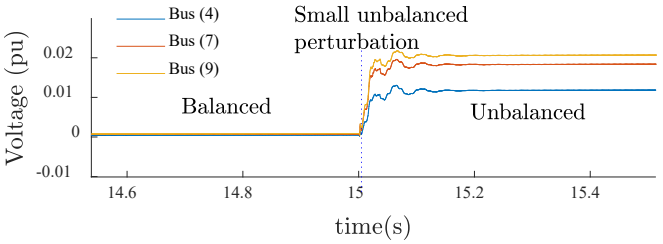

Fig. 4. Magnitude of negative-sequence grid voltages using EMT simulation

Per IEEE 2800 standard [34], IBRs can continue to operate if the negative-sequence component of the applicable voltages is below 3% of the nominal voltage for less than 10 seconds, provided that the voltage imbalance is not caused or exacerbated by unbalanced currents from the IBR.

The time step and simulation duration are set to 100 μs and 20 s, respectively. For GFM-IBRs with the BPSC strategy, Fig. 5 displays the active power simulation results, along with the numerical results from the existing model [23] and our proposed model for comparison. The existing dynamic model solely incorporates positive-sequence dq components in the BPSC system and ignores 2ω negative-sequence components.

During the interval t=15–15.2 s, the transient dynamics of active power differ among GFM-IBRs due to each plant's different primary control strategies. Under steady-state unbalanced grid conditions, the dynamics of the proposed model are highly consistent with the EMT simulations. In addition, Fig. 6 shows that the 100% GFM-IBR-dominated system can still provide a path for the flow of 2ω negative-sequence components.

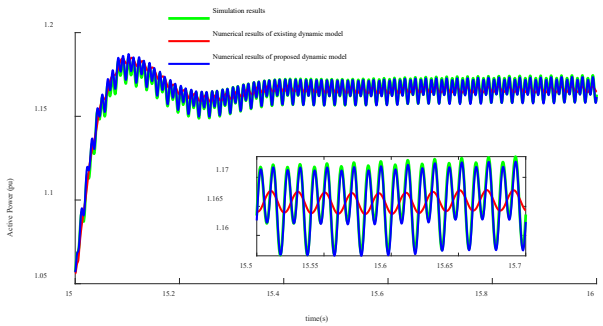

(a) GFM_{VSM}

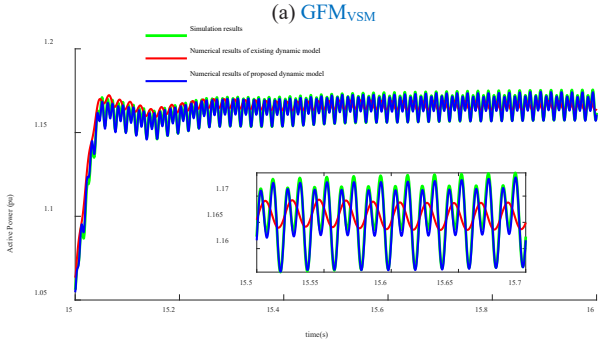

(b) GFM_{droop}

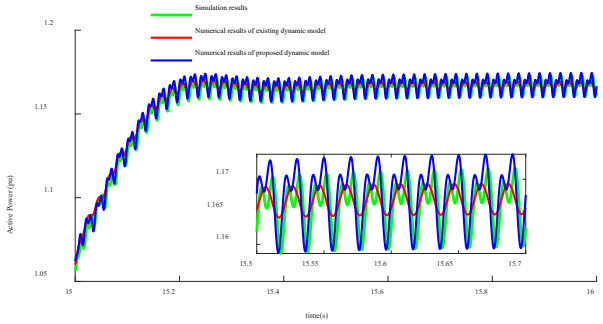

(c) GFM_{dVOC}

Fig. 5. Numerical results and EMT simulation results of active power responses of GFM-IBRs

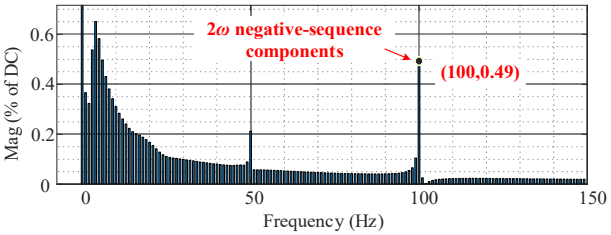

Fig. 6. FFT analysis based on EMT simulation results of active power response of GFM_{VSM}

V. Modal Analysis and EMT Studies for GFM-IBRs under Small Unbalanced Perturbations

A. Oscillatory Modes of GFM-IBRs under Small Unbalanced Perturbations

Based on the state-space matrix derived from the proposed dynamic model, the eigenvalue-based stability assessment (EBSA) is used to study the impacts of control settings and negative-sequence control solutions on oscillatory modes dominated by 2ω negative-sequence components. Oscillatory modes of the GFM_{VSM} are filtered out, as shown in Fig. 7.

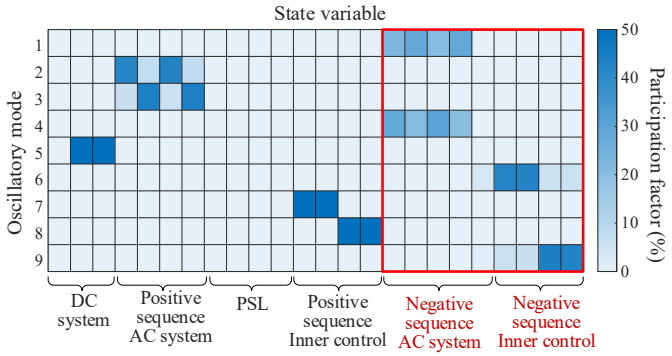

Fig. 7. Participation factors of GFM_{VSM}

In Fig. 7, participation factors are employed to identify the dominant variables. For illustration, the dominant variables are defined as the state variables that exhibit a participation factor exceeding 25%. The eigenvalue λ, damping ratio δ, oscillation frequency f, and dominant variables are listed in Table I.

TABLE I
OSCILLATORY MODES OF GFM_{VSM}

Mode	Λ	δ	f/Hz	Dominant Variables
1	**-1719±2524i**	**0.56**	**401.82**	$\Delta \boldsymbol{I}_{sdq}^{-}$ $\Delta \boldsymbol{V}_{dq}^{-}$
2	-1931±2264i	0.65	360.45	ΔI_{sd}^{+} ΔV_{d}^{+}
3	-1763±1718i	0.72	273.55	ΔI_{sq}^{+} ΔV_{q}^{+}
4	**-1976±1457i**	**0.80**	**231.89**	$\Delta \boldsymbol{I}_{sdq}^{-}$ $\Delta \boldsymbol{V}_{dq}^{-}$
5	-7.20±143.7i	0.05	22.88	ΔI_{dc} ΔV_{dc}
6	**-2.17±0.73i**	**0.95**	**0.12**	$\Delta \boldsymbol{x}_{Vdq}^{-}$
7	-2.23±0.0015i	1.00000	0.00025	$\Delta \boldsymbol{x}_{Vdq}^{+}$
8	-1.61±0.0007i	1.00000	0.00012	$\Delta \boldsymbol{x}_{Idq}^{+}$
9	**-1.53±0.0510i**	**0.99945**	**0.00812**	$\Delta \boldsymbol{x}_{Idq}^{-}$

Table I indicates that under the regulation of the GFM control system, the 2ω negative-sequence components would lead to oscillations at various frequencies (0−0.12 Hz, 231 Hz, 225 Hz, 325 Hz, and 402 Hz), thus deteriorating the dynamic performance. This issue is usually hidden by the dynamic model without consideration of negative-sequence components.

For the DC side, there exists an oscillatory frequency of 22.88 Hz that is caused by the DC-link voltage and current, indicating that the DC-link voltage and current exhibit an oscillation at 22.88 Hz. The result is consistent with the FFT analysis of the DC-link voltage using EMT simulation, as shown in Fig. 8.

For the AC side, the oscillatory frequency caused by *dq* voltages and currents is within the range of 224 Hz to 402 Hz. The real parts of these eigenvalues are around -1800, indicating they are significantly distant from the imaginary axis. Hence, their impact on system stability is relatively minimal. The negative-sequence GFM inner control also generates oscillatory modes. The real parts of these eigenvalues are closer to the imaginary axis, potentially affecting the system's stable operation.

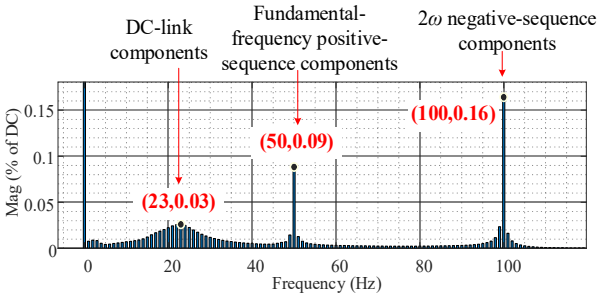

Fig. 8. FFT analysis based on EMT simulation results of the DC-link voltage under small, unbalanced perturbations

B. Impact of Negative-Sequence Control Solutions on Oscillatory Modes under Small Unbalanced Perturbations

For GFM_{VSM} with the PNSC strategy, the negative-sequence voltage at the POC and negative-sequence converter current are shown in Fig. 9. The balanced voltage control effectively suppresses the negative-sequence voltage, while the balanced current control effectively suppresses the negative-sequence current.

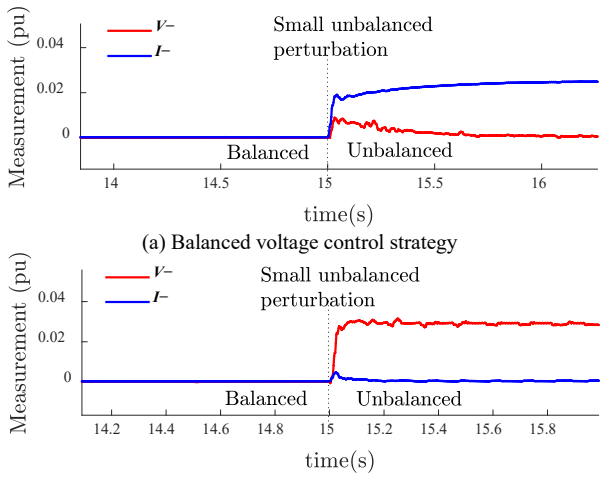

(a) Balanced voltage control strategy

(b) Balanced current control strategy

Fig. 9. EMT simulation results with negative-sequence control solutions in PNSC

For comparison, the oscillatory modes dominated by $\Delta\boldsymbol{x}_{\bar{V}dq}$ and $\Delta\boldsymbol{x}_{\bar{I}dq}$ under the original BPSC and negative-sequence control solutions are shown in Fig. 10. Since there are no negative-sequence voltages within the balanced current control loop, the oscillatory modes dominated by$\Delta x_{\bar{V}dq}$ do not exist under the balanced current control. By using the balanced current control and balanced voltage control strategies, the oscillatory modes shifted to the left. The imaginary part of modes is reduced to zero under the regulation of negative-sequence control solutions. Hence, for the oscillatory modes dominated by $\Delta\boldsymbol{x}_{\bar{V}dq}$ and $\Delta\boldsymbol{x}_{\bar{I}dq}$, using the negative-sequence control solutions increases the damping ratio while reducing the oscillation frequency. This indicates that the additional negative-sequence control solution can eliminate the oscillation, thus improving the control damping of GFM-IBRs.

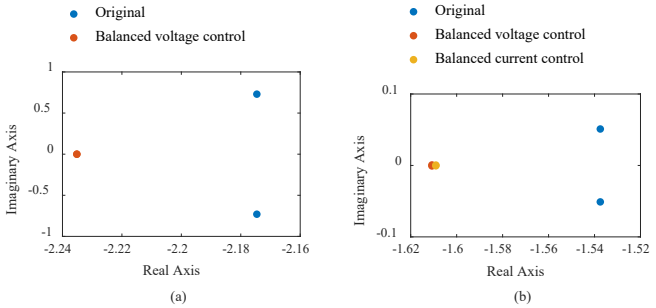

Fig. 10. Oscillatory modes dominated by negative-sequence components under BPSC and PNSC strategies: (a) Modes dominated by $\Delta\boldsymbol{x}_{\bar{V}dq}$; (b) Modes dominated by $\Delta\boldsymbol{x}_{\bar{I}dq}$.

VI. Conclusion

This paper introduces a novel generic decoupled-sequence dynamic model for GFM-IBRs, providing crucial insights into the behavior of 2ω negative-sequence components within the GFM BPSC system under small, unbalanced perturbations. The modal analysis and EMT studies of GFM-IBR-dominated systems reveal several significant findings:

1. Impact of Negative Sequence Components: The 2ω negative-sequence components induce undesirable oscillations across various frequencies, substantially degrading system dynamic performance. This critical effect is often overlooked in conventional dynamic models that neglect negative-sequence components.
2. Effectiveness of Negative-Sequence Control: Implementing balanced current and voltage control strategies shifts oscillatory modes leftward and reduces their imaginary components to zero. This finding suggests the adoption of supplementary negative-sequence controls in GFM-IBRs to enhance control damping under small, unbalanced perturbations.

The proposed model and analysis method provide a powerful methodology for understanding and mitigating the impacts of negative-sequence behavior on system dynamics in GFM-IBR-dominated grids. While this study employs EBSA to focus on oscillatory mode analysis rather than instability mechanisms, it lays a foundation for future research. In this paper, we focus on the oscillations caused by GFM inner controls and the impacts of negative sequence components on system responses. The coupling effects between the sequence components and the frequency dynamics will be also considered in future research.

VII. Appendix

TABLE AI
PARAMETER CONFIGURATION OF GFM-IBRS

Parameter	Value	Parameter	Value
N	200	(k_{pvac}, k_{ivac})	(0.001, 0.0021)
(T_{dc}, k_{Vdc})	(0.05 s, 0.83)	(k_{pv}, k_{iv})	(0.52,232.2)
ω_n	314 rad/s	(k_{pi}, k_{ii})	(0.73, 0.0059)
ω_f	31.4 rad/s	(P_{set}, Q_{set})	(1 pu, 0 pu)
(D_p, J)	(1.01e5, 2.02e3)	(V_{set}, V_{dcset})	(1 pu, 2.45 kV)
(κ_1, κ_2)	(0.0209, 1.39e3)	m_p	3.14e-8
(R_c, L_c)	(5e-6 Ω, 1e-6 H)	(C_{dc}, C_f)	(1.6 F, 0.06 F)
T_{rm}	230 kV /13.8 kV	T_{ru}	13.8 kV/1 kV

In Table AI, T_{rm} and T_{ru} denote the ratio of the main IBR transformer (Yg/D1) and IBR unit transformer (D1/Yg), respectively. This paper focuses on the IBR control dynamics and system-level responses. We model the lines with their pi equivalents. The three-phase transformer (two windings) is the library element in Simulink.

VIII. References

[1] Y. Li, Y. Gu, and T. C. Green, "Revisiting Grid-Forming and Grid-Following Inverters: A Duality Theory," *IEEE Trans. Power Syst.,* vol. 37, no. 6, pp. 4541-4554, 2022.

[2] H. Zhang, W. Xiang, W. Lin, and J. Wen, "Grid Forming Converters in Renewable Energy Sources Dominated Power Grid: Control Strategy, Stability, Application, and Challenges," *Journal of Modern Power Systems and Clean Energy,* vol. 9, no. 6, pp. 1239-1256, 2021.

[3] S. Badakhshan, J. Rahman, and J. Zhang, "Black Start of Coastline Power Networks From Grid-Forming Ship-to-Grid Services," *IEEE Trans. Smart Grid*, vol. 15, no. 2, pp. 1670-1679, 2024.

[4] A. Tayyebi, D. Gross, A. Anta, F. Kupzog, and F. Dorfler, "Frequency Stability of Synchronous Machines and Grid-Forming Power Converters," *IEEE Trans. Emerg. Sel. Topics Power Electron.*, vol. 8, no. 2, pp. 1004-1018, 2020.

[5] Y. Lin, J. Eto, B. Johnson, J. Flicker, R. Lasseter, H. Pico, G. Seo, B. Pierre, and A. Ellis "Research Roadmap on Grid-Forming Inverters," NREL, United States, 2020. [Online]. Available: https://www.osti.gov/biblio/1721727

[6] M. A. Awal, M. R. K. Rachi, H. Yu, I. Husain, and S. Lukic "Double Synchronous Unified Virtual Oscillator Control for Asymmetrical Fault Ride-Through in Grid-Forming Voltage Source Converters," *IEEE Trans. Power Electron.*, vol. 38, no. 6, pp. 6759-6763, 2023.

[7] S. Yazdani, M. Ferdowsi, M. Davari, and P. Shamsi, "Advanced Current-Limiting and Power-Sharing Control in a PV-Based Grid-Forming Inverter Under Unbalanced Grid Conditions," *IEEE Trans. Emerg. Sel. Topics Power Electron.*, vol. 8, no. 2, pp. 1084-1096, 2020.

[8] N. Baeckeland, D. Venkatramanan, M. Kleemann, and S. Dhople, "Stationary-Frame Grid-Forming Inverter Control Architectures for Unbalanced Fault-Current Limiting," *IEEE Trans. Energy Convers.*, vol. 37, no. 4, pp. 2813-2825, 2022.

[9] D. Li, Y. Su, F. Wang, M. Olama *et al.*, "Power Flow Models of Grid-Forming Inverters in Unbalanced Distribution Grids," *IEEE Trans. Power Syst.*, vol. 39, no. 2, pp. 4311-4322, 2024.

[10] B. Mahamedi and J. E. Fletcher, "The Equivalent Models of Grid-Forming Inverters in the Sequence Domain for the Steady-State Analysis of Power Systems," *IEEE Trans. Power Syst.*, vol. 35, no. 4, pp. 2876-2887, 2020.

[11] M.-A. Nasr and A. Hooshyar, "Controlling Grid-Forming Inverters to Meet the Negative-Sequence Current Requirements of the IEEE Standard 2800-2022," *IEEE Trans. Power Del.*, vol. 38, no. 4, pp. 2541-2555, 2023.

[12] C. Li, Y. Huang, Y. Wang, A. Monti, Z. Wang, and W. Zhong, "Modelling and small signal stability for islanded microgrids with hybrid grid-forming sources based on converters and synchronous machines," *International Journal of Electrical Power & Energy Systems*, vol. 157, p. 109831, 2024.

[13] Y. Li, L. Fu, Q. Li, W. Wang, Y. Jia, and Z. Y. Dong, "Small-signal modelling and stability analysis of grid-following and grid-forming inverters dominated power system," *Global Energy Interconnection*, vol. 6, no. 3, pp. 363-374, 2023.

[14] A. Singh, V. Debusschere, N. Hadjsaid, X. Legrand, and B. Bouzigon, "Slow-Interaction Converter-Driven Stability in the Distribution Grid: Small-Signal Stability Analysis With Grid-Following and Grid-Forming Inverters," *IEEE Trans. Power Syst.*, vol. 39, no. 2, pp. 4521-4536, 2024.

[15] R. Pan, D. Liu, S. Liu, J. Yang, L. Kou, and G. Tang, "Stability Comparison Between Grid-forming and Grid-following Based Wind Farms Integrated MMC-HVDC," *Journal of Modern Power Systems and Clean Energy*, vol. 11, no. 4, pp. 1341-1355, 2023.

[16] C. Yang, L. Huang, H. Xin, and P. Ju, "Placing Grid-Forming Converters to Enhance Small Signal Stability of PLL-Integrated Power Systems," *IEEE Trans. Power Syst.*, vol. 36, no. 4, pp. 3563-3573, 2021.

[17] U. Markovic, O. Stanojev, P. Aristidou, E. Vrettos, D. Callaway, and G. Hug, "Understanding Small-Signal Stability of Low-Inertia Systems," *IEEE Trans. Power Syst.*, vol. 36, no. 5, pp. 3997-4017, 2021.

[18] H. Wu and X. Wang, "Small-Signal Modeling and Controller Parameters Tuning of Grid-Forming VSCs With Adaptive Virtual Impedance-Based Current Limitation," *IEEE Trans. Power Electron.*, vol. 37, no. 6, pp. 7185-7199, 2022.

[19] J. Yu, Y. Qi, H. Deng, X. Liu, and Y. Tang, "Evaluating Small-Signal Synchronization Stability of Grid-Forming Converter: A Geometrical Approach," *IEEE Trans. Ind. Electron.*, vol. 69, no. 9, pp. 9087-9098, 2022.

[20] P. Liu, X. Xie, and J. Shair, "Adaptive Hybrid Grid-Forming and Grid-Following Control of IBRs with Enhanced Small-Signal Stability under Varying SCRs," *IEEE Trans. Power Electron.*, pp. 1-5, 2024.

[21] F. Zhao, X. Wang, and T. Zhu, "Power Dynamic Decoupling Control of Grid-Forming Converter in Stiff Grid," *IEEE Trans. Power Electron.*, vol. 37, no. 8, pp. 9073-9088, 2022.

[22] L. Zhao, Z. Jin, and X. Wang, "Small-Signal Synchronization Stability of Grid-Forming Converters with Regulated DC-Link Dynamics," *IEEE Trans. Ind. Electron.*, vol. 70, no. 12, pp. 12399-12409, 2023.

[23] D. A. Aragon, E. Unamuno, S. Ceballos, and J. A. Barrena, "Comparative small-signal evaluation of advanced grid-forming control techniques," *Electric Power Systems Research*, vol. 211, p. 108154, 2022.

[24] S. Eberlein and K. Rudion, "Impact of Inner Control Loops on Small-Signal Stability and Model-Order Reduction of Grid-Forming Converters," *IEEE Trans. Smart Grid*, vol. 14, no. 4, pp. 2812-2824, 2023.

[25] M. H. Ravanji, D. B. Rathnayake, M. Z. Mansour, and B. Bahrani, "Impact of Voltage-Loop Feedforward Terms on the Stability of Grid-Forming Inverters and Remedial Actions," *IEEE Trans. Energy Convers.*, vol. 38, no. 3, pp. 1554-1565, 2023.

[26] J. Liu, Y. Xia, W. Wei, Q. Feng, and P. Yang, "Effect of Control Damping on Small-Signal Stability of Grid-Forming VSCs Considering Interaction Between Inner and Outer Loops," *IEEE Trans. Power Electron.*, pp. 1-10, 2024.

[27] J. Yu, S. Wang, Z. Liu, J. Li, J. Liu, and J. Shang, "Accurate Small-Signal Terminal Characteristic Model and SISO Stability Analysis Approach for Parallel Grid-Forming Inverters in Islanded Microgrids," *IEEE Trans. Power Electron.*, vol. 38, no. 5, pp. 6597-6612, 2023.

[28] Z. Zhao, X. Luo, J. Xie, S. Gong, J. Guo, Q. Ni, C. Lai, P. Yang, and L. Lai, "Decentralized Grid-Forming Control Strategy and Dynamic Characteristics Analysis of High-Penetration Wind Power Microgrids," *IEEE Trans. Sustain. Energy*, vol. 13, no. 4, pp. 2211-2225, 2022.

[29] M. A. Awal, S. Cen, M. R. K. Rachi, H. Yu, S. Schröder, and I. Husain, "Modeling, Analysis, and Design for Small-Signal Stability in Sequence-Decomposed Grid-Forming Control," *IEEE Trans. Ind. Appl.*, vol. 60, no. 1, pp. 865-875, 2024.

[30] S. J. Yague, A. Garcia-Cerrada, and P. Palacin Farre, "Comparison Between Modal Analysis and Impedance-based Methods for Analysing Stability of Unbalanced Microgrids with Grid-forming Electronic Power Converters," *Journal of Modern Power Systems and Clean Energy*, vol. 11, no. 4, pp. 1269-1281, 2023.

[31] P. Rodriguez, J. Pou, J. Bergas, J. I. Candela, R. P. Burgos, and D. Boroyevich, "Decoupled Double Synchronous Reference Frame PLL for Power Converters Control," *IEEE Trans. Power Electron.*, vol. 22, no. 2, pp. 584-592, 2007.

[32] E. Avdiaj, J. A. Suul, S. D. Arco, and L. Piegari,"A Current Controlled Virtual Synchronous Machine Adapted for Operation under Unbalanced Conditions," in 2020 9th International Conference on Renewable Energy Research and Application (ICRERA), 27-30 Sept. 2020.

[33] E. B. Avdiaj, S. D'Arco, L. Piegari, and J. A. Suul, "Negative Sequence Control for Virtual Synchronous Machines Under Unbalanced Conditions," *IEEE Trans. Emerg. Sel. Topics Power Electron.*, vol. 10, no. 5, pp. 5670-5685, 2022.

[34] "*IEEE Standard for Interconnection and Interoperability of Inverter-Based Resources (IBRs) Interconnecting with Associated Transmission Electric Power Systems*," IEEE Std 2800-2022, pp. 1-180, 2022